Near-surface velocity estimation for a realistic 3D synthetic model

Xukai Shen

ABSTRACT

I performed data-domain wave-equation tomography for a realistic synthetic near-surface model. From a starting model that misses some large scale velocity features as well as some small scale velocity features, both traveltime tomography and waveform tomography were performed. First-break traveltime tomography using wave equation not only results in correct updates of large scale velocity structure, but also gives hints of small scale velocity structures. The tomography result can be further refined by refraction waveform tomography. Refraction waveform tomography pin-point the location of small scale velocity features by using the waveform information in addition to the traveltime information. However, direct refraction waveform tomography without traveltime tomography can not resolve the missing large velocity features in the starting model, and easily converges to a local minima.

INTRODUCTION

Conventionally, people use ray-based methods (Hampson and Russell, 1984; Olson, 1984; White, 1989) to derive near-surface velocity. Such smooth solutions may be adequate for areas with simple near-surface velocity structures, but in geologically complex areas, smooth velocities are not accurate enough for imaging deeper reflectors (Marsden, 1993; Bevc, 1995; Hindriks and Verschuur, 2001). In such cases, data-domain wave-equation tomography (Tarantola, 1984; Pratt et al., 1998; Mora, 1987; Luo and Schuster, 1991) tends to give more accurate results (Ravaut et al., 2004; Sheng et al., 2006; Sirgue et al., 2009) by simulating finite-frequency seismic wave propagation.

Data-domain wave-equation tomography methods update velocity using mismatches between observed data and modeled data. The mismatches usually include traveltime (first-order) and waveform (second-order) mismatches. Both traveltime and waveform mismatches are used by Full Waveform Inversion (FWI) (Tarantola, 1984; Pratt et al., 1998; Mora, 1987), leading to high-resolution results but requiring an accurate starting model. On the other hand, Wave-equation Traveltime Inversion (WTI) (Luo and Schuster, 1991) estimates velocity model by minimizing only the traveltime difference between observed data and modeled data using the wave equation. As a result, WTI differs from FWI in two ways: first, WTI is not affected by bad starting models with

cycle skipping; second, WTI results tend to have low resolution. However, the low-resolution result from WTI can be a good starting model, and subsequent FWI can obtain a high-resolution result (Shen et al., 2012).

In this paper, I examine the resolution of first-break traveltime wave-equation tomography and refraction waveform tomography, using a realistic near-surface model with complex velocity structures. The model contains velocity features of various spatial extend, making it a good candidate for testing tomography resolution. First I will review data-domain wave-equation tomography methodology, then I will show why ray is unfavorable in such setting, finally I will compare and analyze tomography results.

REVIEW OF DATA-DOMAIN EARLY ARRIVAL WAVE-EQUATION TOMOGRAPHY

Data-domain wave-equation tomography updates velocity or earth model in an iterative fashion by minimizing the difference between synthetically modeled data and recorded data. The tomography scheme can be summarized by the following pseudo code:

Algorithm 1 Pseudo code of data-domain wave-equation tomography

for iteration =1,n **do**
  Calculate gradient of objective function regarding model parameters.
  Calculate update direction using the current gradient (and/or previous gradients).
  Calculate steplength of the update direction.
  Update model.
end for

Data-domain early arrival wave-equation tomography, as the name suggests, tries to model and match only early (temporal) arrivals in recorded data. Since early arrivals mainly travels through near-surface before returning to the surface, it is the ideal candidate when we are only inverting for near-surface velocity. Early arrivals include refractions, diving waves and shallow reflections. While shallow reflections can be used for near-surface velocity analysis(Shen, 2013), the tomography carried out in this paper used refraction and diving waves only. As will be shown in the example, to recover both large scale and small scale velocity features, both traveltime and waveform of refraction/diving waves are needed.

Using waveform or traveltime in the tomography is achieved by using different objective functions. More specifically, waveform tomography uses objective functions that subtract modeled data from recorded data, usually with some amplitude correction term to account for the amplitude difference caused by non-velocity factors(Shen, 2010). Traveltime tomography, on the other hand, uses objective functions that measure the traveltime difference between recorded and observed data, this can be done

by one of the two options: 1. picking the time lag that maximize the correlation between recorded data and observed data; 2; picking the traveltime of corresponding events (such as first-breaks) in both recorded data and observed data, then subtract the two picks.

Using waveform and/or traveltime of recorded data in the tomography naturally leads to the choice of time-domain(Mora, 1987) tomography scheme over frequency-domain scheme(Pratt et al., 1998) . Traditional time-domain schemes are very computationally expensive for two reasons: first, it involves iterative forward and backward two-way wavefield propagation; second, to compute velocity update direction, at least one of the wavefield needs to be saved. Because wavefields in large-scale 3D application can require terabytes of storage, I/O can be a non-trivial bottleneck. While computational power is growing very fast, it is less so for the memory size of computers. As shown in the pseudo code in Appendix A, using random boundaries can greatly reduce the memory requirement, hence eliminating the I/O bottleneck.

COMPLEX VELOCITY STRUCTURE AND RAY BEHAVIOR

In the history of geophysical prospecting, people have identified and categorized many types of near-surface velocity features. However, to combine them into a realistic near-surface velocity model, it is better to generate those features via geological oriented process. Robert Clapp proposed one way of doing this in the last SEP report(Clapp, 2013), which was used to generate the near-surface velocity model in this paper.

The velocity model is generated by a series of geological processes. The most frequently used process is deposit, where a layer of constant thickness velocity is deposited onto the top of the current model, within the layer there are also fine layering and random lateral velocity variations. Both features are part of the true model (figure 1), and both are removed from the starting model. Depositing layers create a simple model that can be made more complex. More specifically, the simple model can be made more complex by certain "morphing" processes such as uplift (figure 2), compact and faulting. Those processes create macro velocity features, micro velocity features can be created by erosion processes. Current version of the software is capable of creating channel or "bowl" erosion, both types of which are used in creating the true model, but not the starting model for tomography. The velocity model created by the combination of all those processes are realistically complicated (figure 3).

Ray based methods have a very difficult time to deal with such complicated near-surface model. To illustrate this, I took a 2D slice of the 3D model, then performed three scenarios of ray tracing on the 2D slice (figure 4). All the scenarios use the same source to propagate four rays, each ray propagate ten seconds or hit the earth surface, whichever came first. The take-off angle of rays starts at forty-nine degrees from vertical down, with five and an half degrees increment. The only difference

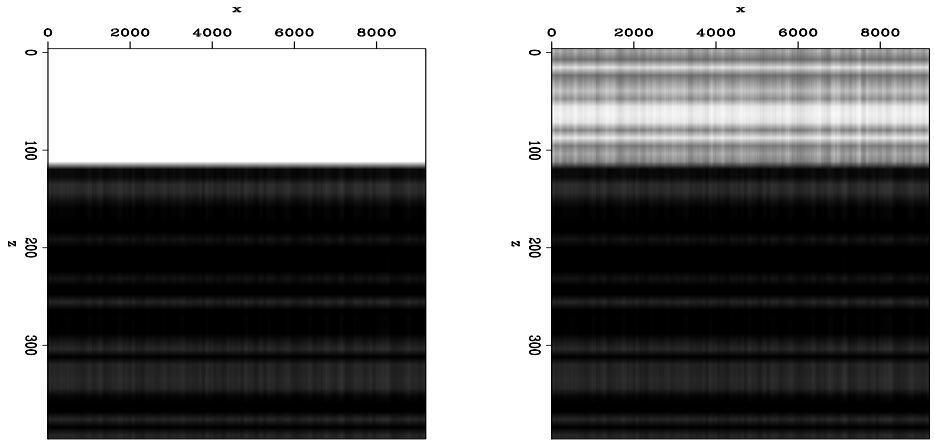

Figure 1: Velocity model building process, left: before deposition; right: after deposition. [**ER**]

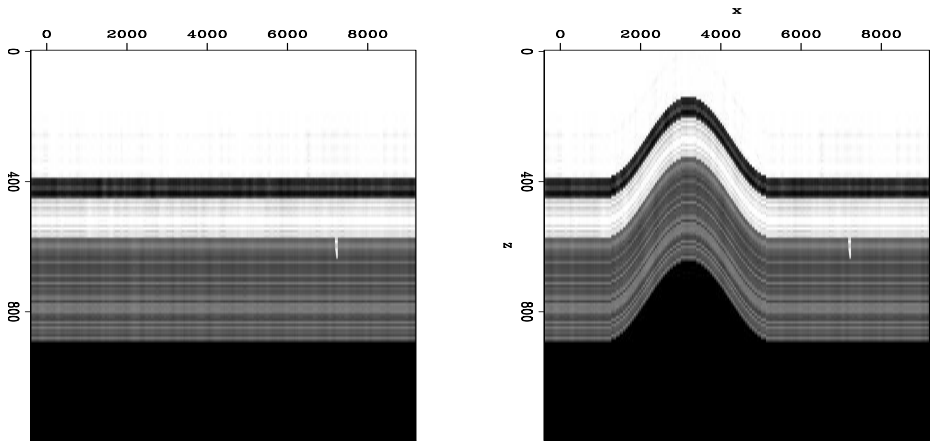

Figure 2: Velocity model building process, left: before uplift; right: after uplift. [**ER**]

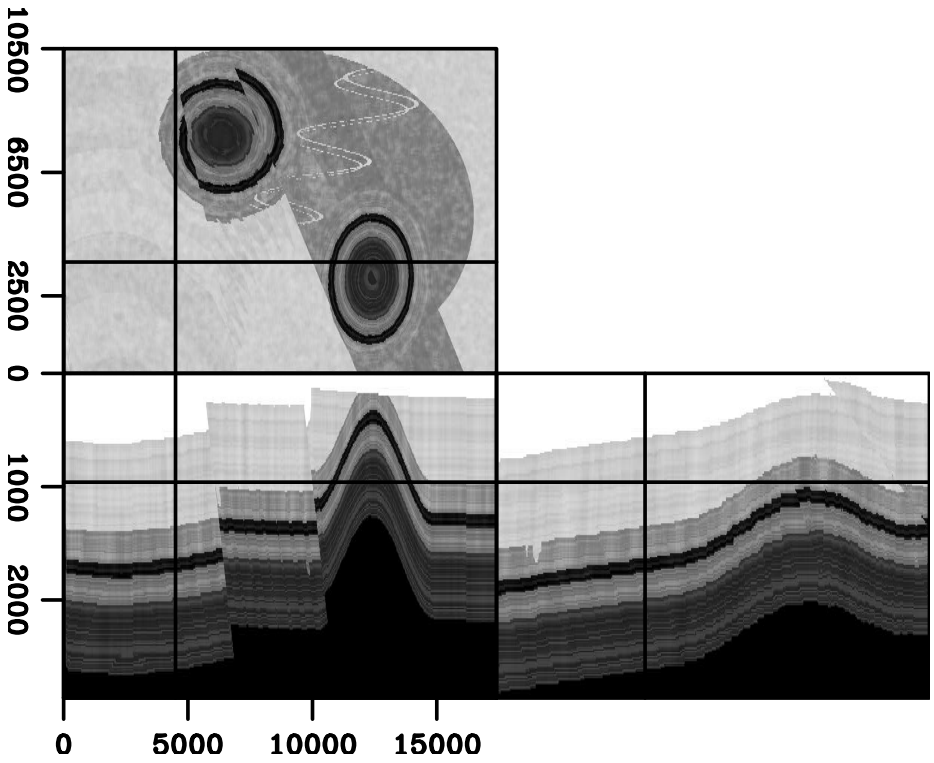

Figure 3: True velocity model for tomography. [**ER**]

being the propagation time interval, where the first scenario use one milli-second interval, and the second and the third scenario use half and quarter Milli-second, respectively. Change of the time interval lead to slight lateral shift when rays hit the first interface. However, such small change in lateral arrival point translate into huge different in the later ray path. This is particularly obvious in the diving/refraction rays. Diving/refraction rays in such complicated velocity model is highly non-linear with ray parameters. Such non-linearity will be much worse in the full 3D model, making it completely unsuitable for high-resolution tomography. The starting model (figure 5) is created by using most of the steps that created the true model. All the depositing steps are used, but fine layering, lateral variation of velocity within each layer and thin layer of high velocity are removed. All the "morphing" are applied exactly the same way. All the erosion steps are skipped. Also the model created by those steps are smoothed before using as input to tomography. Such a starting model simulates ray-based near-surface tomography result, where the model is usually smooth and lacks lateral resolution.

TOMOGRAPHY AND RESULTS

Given the complicated true model, particularly the depth of various features, synthetic survey is designed such that most of the features are illuminated by diving

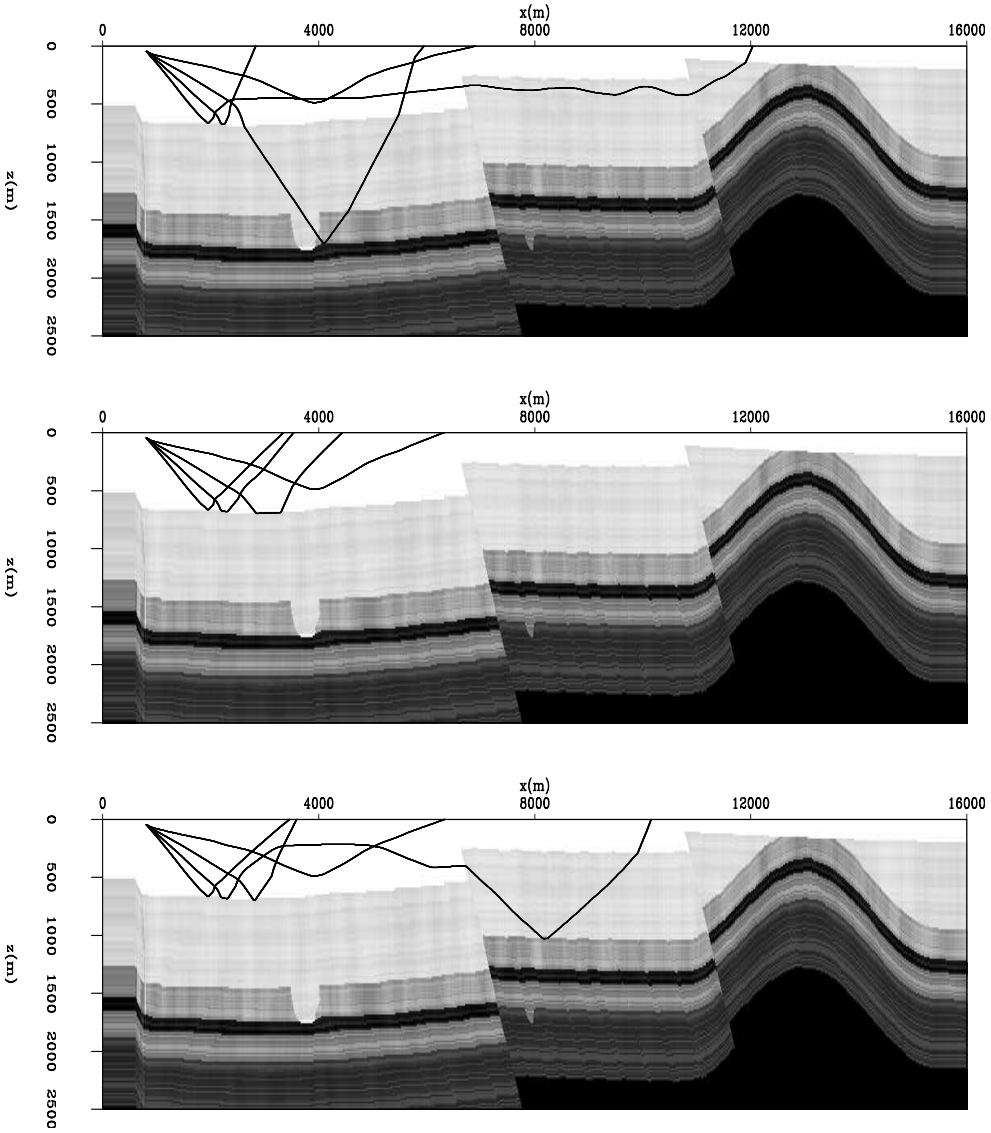

Figure 4: Ray tracing through the 2d slice of the true Velocity model with top: 1ms time interval; middle:0.5 ms time interval;bottom:0.25 ms time interval. [**ER**]

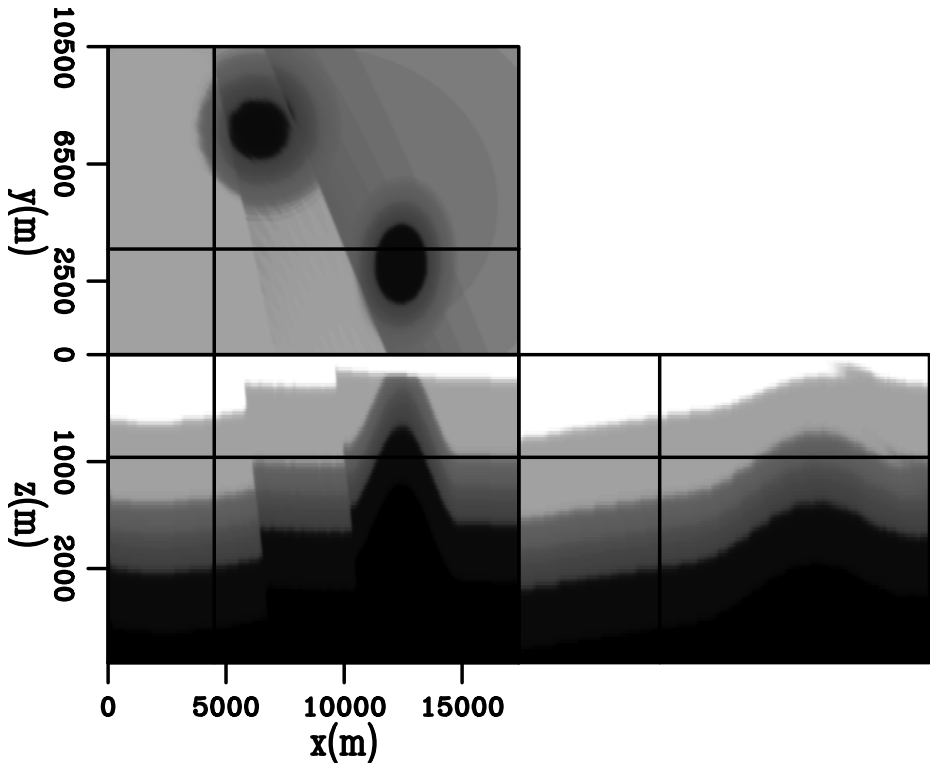

Figure 5: Starting velocity model for tomography. [**ER**]

waves/refractions. The survey simulates a typical cross-spread land survey setting. Source lines are along cross-line direction. Receiver lines are along inline direction, and are orthogonal to source lines. Source spacing is 120m along the cross-line direction, and 390m along the inline direction. Each shot point is centered in a rectangular patch of receivers. Receivers offset range from -5.1km to 5.1km in the inline direction, with 30m spacing, and -2km to 2km in the crossline direction, with 180m spacing. Since we are only interested in using diving wave/refractions, the recording time was only 3.5 seconds. A total number of 3240 shots are modeled with each shot contains up to 7840 traces. All the data are modeled on 15 m grid spacing in x, y and z, with time sampling of 3 ms. The total amount of data are more than 100 GB.

To recover lateral velocity variation from starting model, it is important to choose data frequency that contains information of those velocity variations. I use the quarter-wavelength rule to select my temporal frequency. The rule states that seismic wave with spatial wavelength of x can resolve spatial velocity feature that is equal or larger than $x/4$. This empirical rule is very useful here since the true model contains not only small scale lateral velocity variations, but also two sinusoidal channels that are very close to each other in some places. To make sure we can invert for those small scale velocity variations, a Ricker wavelet of 12Hz was used for both modeling and tomography. The small scale velocity variation is on the order of ten numerical grids, hence for computational efficiency, inversion were carried out on $30m$ spacing

in x,y and z, with time sampling of 6 ms.

Three tomography tests are performed, the first one is the wave-equation traveltime tomography by minimizing the first break traveltime differences between observed data and modeled data. The second and third are both waveform tomography by minimizing refraction/diving waveform differences between observed data and modeled data. The two waveform tomography use different starting models, one uses traveltime tomography result, the other uses the starting model for traveltime tomography.

Traveltime tomography is less sensitive to cycle-skipping than waveform tomography. As a result, relatively bold steplength search is performed for each iteration. A total number of 10 iterations were run. The inverted model is in figure 6, it is still smooth compare with the true model. However, a close comparison to the starting model shows that most velocity features already start to appear. For example Given the velocity of about 2.5km/s where the two river channels are at, the quarter-wavelength rule suggest that the 12Hz peak frequency wavelet can detect velocity features down to about 50m. Since the channels have width and depth that are bigger than 100m, they can be resolved (figure 6. At the same time, other bigger velocity features such as lateral velocity variation, high velocity layer, and "bowl" type erosion are resolved as well. However, resolving in the content of traveltime tomography means the bulk of the velocity features start to appear, but not the exact boundaries of velocity features. Resolving the boundary requires us to at least correct the second order data misfit-the waveforms.

For the waveform tomography, since waveform dependency on velocity or slowness is less linear compare to that of traveltime, both waveform tomography tests use a cautious steplength search. This result in smaller steplength per iteration and more iterations for tomography. Thirty iterations were run for waveform tomography from traveltime tomography result. Forty iterations were run for waveform tomography from starting model. This way, both waveform tomography results are derived using the same amount of computation, and comparison makes more sense from practical point of view. The other practicality comes into the choice of data for waveform tomography. Both waveform tomography used all the refraction/diving wave data rather than only using first break waveforms. Using the extra non-firstbreak refraction/diving wave barely increase computation while brings much more information into tomography, leading to better tomography results.

Waveform tomography result starting from traveltime tomography model is in figure 7. The resolution is much higher than that from traveltime tomography. Boundaries of all the velocity features become better defined. Even the two channels can be recognized where they are close to each other. Tomography from the starting model (figure 8) resolves the boundaries of velocity structures well, however, due to its inability of updating the bulk of the velocity structures, it did not converge to the correct velocity model. This is particularly obvious in the inline section, where direct waveform tomography solves part of the "bowl" type erosion boundary, yet is unable to solve the interior of the erosion.

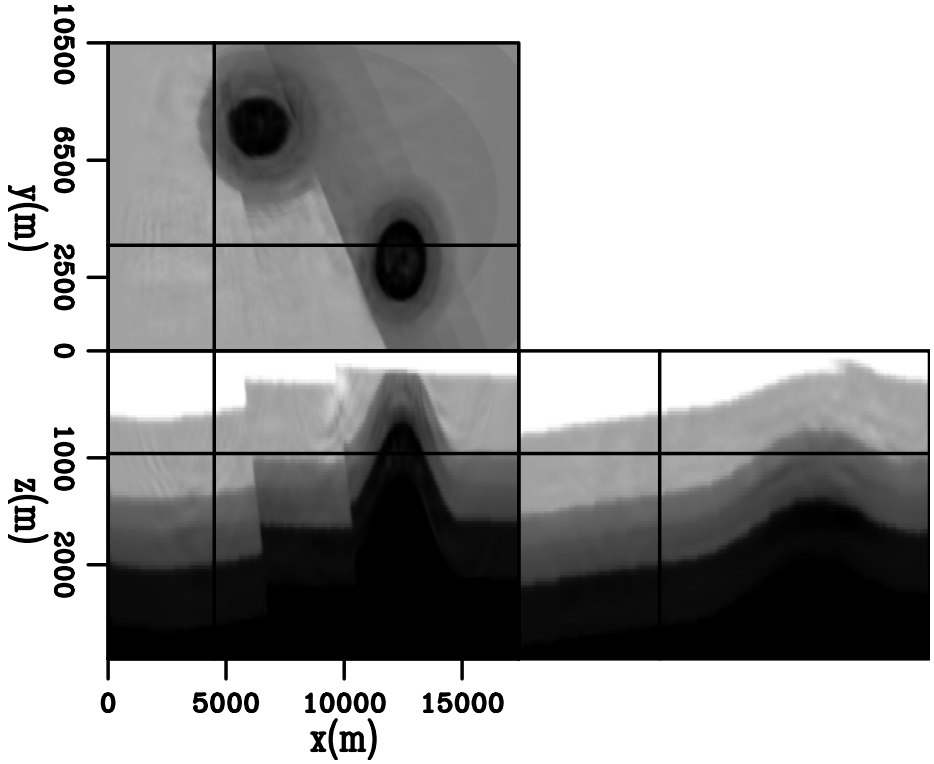

Figure 6: Traveltime tomography result. [**CR**]

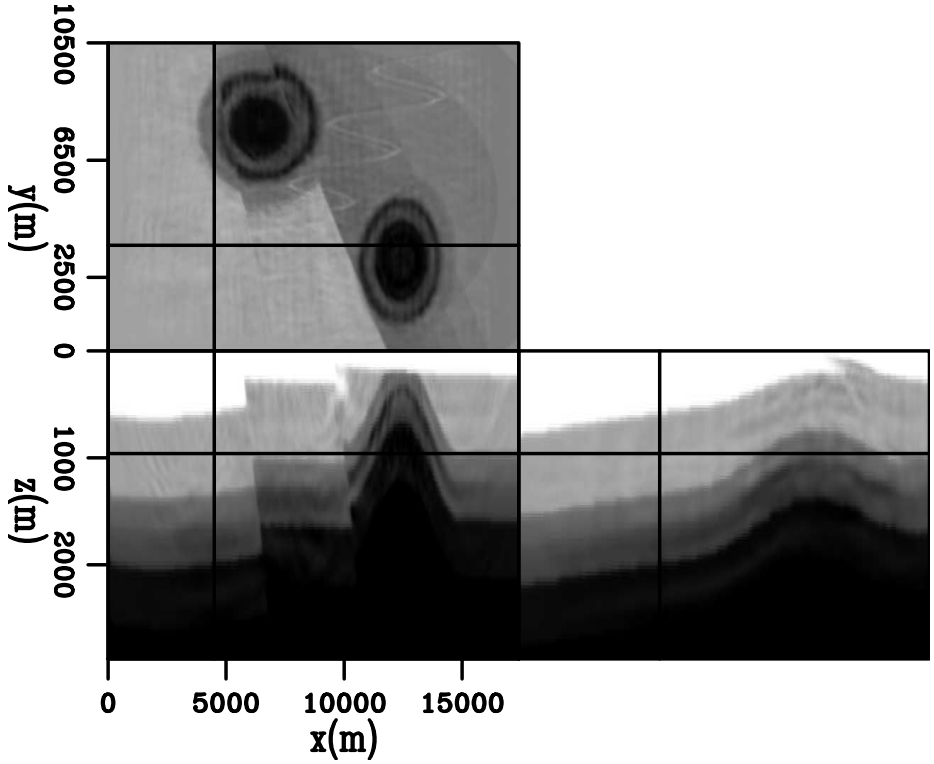

Figure 7: Waveform tomography result using traveltime result as starting model. [**CR**]

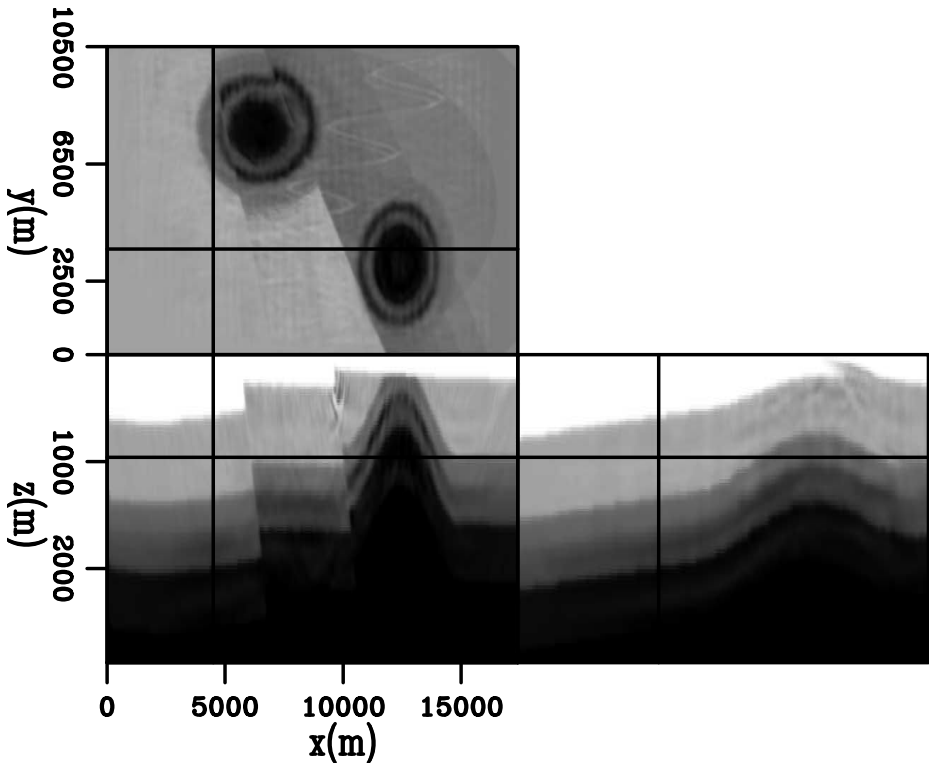

Figure 8: Waveform tomography result using the starting model. [**CR**]

CONCLUSION

Wave-equation based methods perform better than ray based methods in building near-surface velocity model for geologically complex area. Physically, wave propagation is a better approximation than its high frequency approximations; numerically, rays easily become unstable with complex velocity structure. When both traveltime wave-equation tomography and waveform wave-equation tomography are performed, traveltime is better at resolving the bulk of velocity structures, while waveform is better at accurately define the boundaries of velocity structures. However, Waveform tomography can not converge to the true model if the bulk of the velocity structures are not resolved.

REFERENCES

Bevc, D., 1995, Imaging under rugged topography and complex velocity structure: SEP Ph.D Thesis.

Clapp, R. G., 2013, Synthetic model building using a simplified basin modeling approach: SEP Report, **149**.

Hampson, D. and B. Russell, 1984, First-break interpretation using generalized linear inversion: Journal of CSEG, **20**, 40–54.

Hindriks, C. and D. Verschuur, 2001, Common focus point approach to complex near surface effects: SEG Expanded Abstracts.

Luo, Y. and G. T. Schuster, 1991, Wave-equation traveltime inversion: Geophysics, **56**, 645–653.

Marsden, D., 1993, Statics corrections-a review: The Leading Edge.

Mora, P., 1987, Elastic wavefield inversion: SEP Ph.D Thesis.

Olson, K. B., 1984, A stable and flexible procedure for the inverse modelling of seismic first arrivals: Geophysical Prospecting, **37**, 455–465.

Pratt, R. G., C. Shin, and G. Hicks, 1998, Gauss-Newton and full Newton methods in frequency domain seismic waveform inversion: Geophysical Journal International, **133**, 341–362.

Ravaut, C., S. Operto, L. Improta, J. Virieux, A. Herrero, and P. Dell'Aversana, 2004, Multiscale imaging of complex structures from multifold wide-aperture seismic data by frequency-domain full-waveform tomography: application to a thrust belt: Geophysical Journal International, **159**, 1032–1056.

Shen, X., 2010, Near-surface velocity estimation by weighted early-arrival waveform inversion: SEG Expanded Abstracts.

———, 2013, Anti-noise wave-equation traveltime inversion and application to salt estimation: SEP Report, **149**.

Shen, X., T. Tonellot, Y. Luo, T. Keho, and R. Ley, 2012, A new waveform inversion workflow: Application to near-surface velocity estimation in saudi arabia: SEG Abstracts.

Sheng, J., A. Leeds, M. Buddensiek, and G. T. Schuster, 2006, Early arrival waveform tomography on near-surface refraction data: Geophysics, **71**, U47–U57.

Sirgue, L., O.I.Barkved, J. V. Gestel, O. Askim, and R. Kommedal, 2009, 3d waveform inversion on valhall wide-azimuth obc: EAGE 71th Conference.

Tarantola, A., 1984, Inversion of seismic reflection data in the acoustic approximation: Geophysics, **49**, 1259–1266.

White, D. J., 1989, Two-dimensional seismic refraction tomogaphy: Geophysical Journal International, **97**, 223–245.

APPENDIX A

PSEUDO CODE FOR GRADIENT CALCULATION USING DIFFERENT BOUNDARY CONDITIONS

Algorithm 2 Pseudo code of gradient calculation using absorbing boundary condition

for $is = 1, ns$ **do**
  Forward wavefield propagation, generate modeled data and record source wavefield;
  Calculate data residual using recorded data and modeled data;
  Reverse-time propagation of residual data, correlate residual wavefield with source wavefield to generate gradient;
end for

Algorithm 3 Pseudo code of gradient calculation using random boundary condition

for $is = 1, ns$ **do**
  forward wavefield propagation using absorbing boundary, generate modeled data, do not record wavefield;
  forward wavefield propagation using random boundary, record last two time slices of source wavefield;
  calculate data residual using recorded data and modeled data;
  reverse time propagation of residual data and source wavefield using random boundary, generate gradient on the fly;
end for